Two-dimensional device simulation program: 2DP

by S. P. Gaur
P. A. Habitz
Y.-J. Park
R. K. Cook
Y.-S. Huang
L. F. Wagner

Mathematical details of a two-dimensional semiconductor device simulation program are presented. Applicability of the carrier transport model to shallow junction bipolar transistors is discussed. Use of this program to optimize device structures in new bipolar technology is illustrated by presenting calculated device characteristics for variations in a few selected process conditions. Software links that automatically transfer data from a two-dimensional process simulation program and to a quasi-three-dimensional device equivalent circuit model generation program are also discussed.

1. Introduction

With the rapid advances in semiconductor technology over the past several decades, the number of devices and circuits per chip is increasing at a remarkable rate. In the present era of very large scale integration, it is becoming increasingly important to use computer-aided semiconductor device analysis and design to shorten the technology design cycle, improve accuracy of design, and reduce design cost. This paper presents details of a mathematical model based on semiconductor device physics that predicts device characteristics so that the output can be used for their equivalent circuit representation. Such predictive models are the only tools available in the early phases of technology development for device and process optimization. However, to be useful it is important that these mathematical models accurately reflect the characteristics of current devices and are capable of analyzing future devices with shrinking dimensions.

An accompanying paper [1] has introduced our mathematical models for process and device simulations and their use in bipolar technology development. The two-dimensional device simulation program described here, 2DP, has evolved to its present form over the last ten years [2–6]. It has been developed as a general-purpose analysis program for semiconductor devices (including merged structures) and has been especially optimized for steady state bipolar structures. An interactive user-oriented program has been developed to automatically create the geometry, doping profile, terminal bias, and other control parameters required as input to the program. Software links have also been developed to automatically receive doping profiles generated by the two-dimensional process simulation program SAFEPRO [7] and to automatically transfer 2DP predicted device terminal characteristics and internal behavior required for equivalent circuit modeling to the model generation program MGP [8].

The physical effects of heavy doping, hot carrier, and velocity overshoot are becoming increasingly important as devices are scaled down to the submicrometer range. For example, as the emitter size of a bipolar transistor becomes smaller, the transistor is operated in a high-injection range due to increased current density, and consequently the device current gain becomes sensitive to heavy doping effects due to carrier-carrier interactions [6]. Review and verification of semiconductor physics and material parameters as modeled in 2DP are an ongoing effort. Device characteristics predicted by 2DP have been verified with measured terminal characteristics on various types of semiconductor devices [5, 6]. Hot carrier and velocity overshoot of carriers in the collector depletion region have

been simulated in one dimension by modifying the semiconductor transport equations [9]. This velocity overshoot effect does not significantly affect the predicted device terminal characteristics of the bipolar transistors discussed in this paper. The applicability of the semiconductor transport equations used in 2DP for the analysis of the shallow junction bipolar transistors considered in this paper has also been established by an alternate modeling approach [10]. Monte Carlo simulation of carrier transport shows that predicted device terminal characteristics increase by no more than 5% due to the velocity overshoot effect.

Section 2 describes the semiconductor device equations and silicon material parameters used in 2DP. Numerical techniques used to solve the mathematical equations and boundary conditions used are also discussed. Use of this program to analyze and optimize bipolar technology devices is presented in Section 3.

2. Model

The set of equations used to simulate steady state carrier transport in bipolar transistors is as follows:

$$F_\psi = \nabla^2\psi + \frac{q}{\varepsilon}(p - n + N_D - N_A) = 0, \quad (1)$$

$$F_n = \nabla J_n + q(G - R) = 0, \quad (2)$$

$$F_p = \nabla J_p - q(G - R) = 0, \quad (3)$$

with auxiliary equations

$$J_n = -q\mu_n n\nabla\phi_n, \quad (4)$$

$$J_p = -q\mu_p p\nabla\phi_p, \quad (5)$$

$$n = n_{i0}\exp[\Delta E_c/kT]\cdot\exp[q(\psi - \phi_n/kT], \quad (6)$$

$$p = p_{i0}\exp[\Delta E_v/kT]\cdot\exp[q(\phi_p - \psi)/kT], \quad (7)$$

$$n_{ie}^2 = n_{i0}\cdot p_{i0}\cdot\exp[\Delta E_g/kT], \quad (8)$$

$$R = R_{SRH} + R_{AUGER}, \quad (9)$$

$$R_{SRH} = (pn - n_{ie}^2)/[\tau_{n0}(p + n_{ie}) + \tau_{p0}(n + n_{ie})], \quad (10)$$

$$R_{AUGER} = (A_n n + A_p p)(pn - n_{ie}^2), \quad (11)$$

$$G = [\alpha_n(E)|J_n| + \alpha_p(E)|J_p|]/q, \quad (12)$$

$$E = -\nabla\psi. \quad (13)$$

Heavy doping effects are taken into account by the Auger recombination term R_{AUGER} and a correction to the intrinsic carrier concentration n_i, as given in (8). ΔE_g in (8) is the "effective bandgap narrowing" which takes into account heavy doping effects such as band tailing, many-body effects, and Fermi-Dirac statistics. Bandgap narrowing parameters, as well as mobility, lifetime parameters, and ionization rates that are assumed in the model, are discussed in the next section.

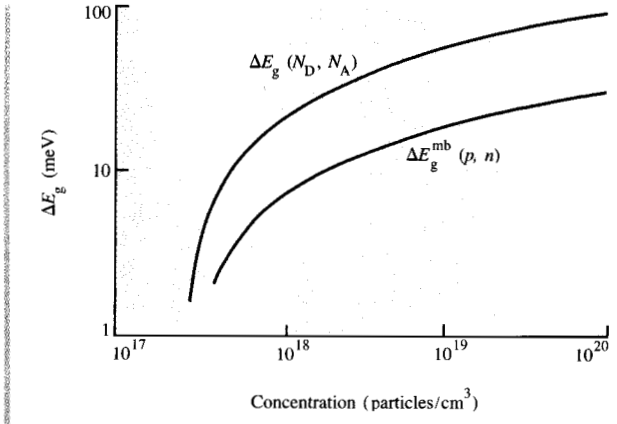

Figure 1

Bandgap narrowing vs concentration. Upper curve is an empirical relation for the total band gapnarrowing (ΔE_g). Lower curve is bandgap narrowing due to many-body effects.

• *Material parameters*

Effective bandgap narrowing is taken to be a function of impurity doping and carrier concentration [6] as given by the following expressions:

$$\Delta E_g = \Delta E_c + \Delta E_v, \quad (14)$$

$$\Delta E_c = \Delta E_c^{bt}(N_D) + \Delta E_c^{bt}(N_A) + \Delta E_c^{mb}(p), \quad (15)$$

$$\Delta E_v = \Delta E_v^{bt}(N_D) + \Delta E_v^{bt}(N_A) + \Delta E_v^{mb}(n), \quad (16)$$

where ΔE_c is the shift in conduction band energy and ΔE_v is the shift in valence band energy. Superscripts bt and mb in (15)–(16) denote band edge shrinkage due to band tailing and many-body effects, respectively. Details of this bandgap narrowing model have been described elsewhere [6]. Briefly, band edge shrinkage due to band tailing is taken to be a function of doping concentration N_D or N_A, while many-body terms consist of an upward shift of valence band due to hole-electron interactions and a downward shift of conduction band due to electron-hole interactions. **Figure 1** shows total bandgap narrowing as a function of doping concentration as it is assumed in this model. Figure 1 also shows the contribution of the many-body terms to the total bandgap shrinkage in the equilibrium condition. This modification to the previous bandgap narrowing model [5] was found necessary for more accurate prediction of transistor current gain at high injection levels.

Various models for carrier mobilities are available in the literature. The mobility model selected here gives the best results when evaluated with hardware consisting of a variety of profiles and geometries. In this model hole mobility μ_p and electron mobility μ_n are taken to be a function of doping ($N = N_D + N_A$) and normalized temperature (T_n) [11] as

given by the following expressions:

$$\mu_p = 54.3\,T_n^{-0.57} + \frac{407\,T_n^{-2.23}}{1 + \left(\dfrac{N}{2.35\cdot 10^{17} T_n^{2.4}}\right)^{0.88\cdot T_n^{-0.146}}}, \tag{17}$$

$$\mu_n = 88\,T_n^{-0.57} + \frac{1252\,T_n^{-2.23}}{1 + \left(\dfrac{N}{1.26\cdot 10^{17} T_n^{2.4}}\right)^{0.88\cdot T_n^{-0.146}}}. \tag{18}$$

The electric field (E) dependence of the mobility [12] is taken into account by the following expression:

$$\mu = \frac{\mu_0(N, T_n)}{\left[1 + \left(\dfrac{E}{E_c}\right)^{\beta}\right]^{1/\beta}}, \tag{19}$$

where

$$\beta = 1.213,$$

$$E_c = \frac{8.34\cdot 10^6 T_n^{-0.52}}{\mu_0} \text{ for holes,}$$

$$E_c = \frac{1.07\cdot 10^7 T_n^{-0.87}}{\mu_0} \text{ for electrons,}$$

and where μ_0 in (19) is the low field mobility value of Eq. (17) or (18).

Lifetime parameters τ_{n0} and τ_{p0} in the Shockley-Read-Hall recombination term R_{SRH} (10) are taken to be equal to 1.0×10^{-6} sec and constant all over the device. Parameters A_n and A_p in the Auger recombination term R_{AUGER} (11) are taken to be equal to 1.4×10^{-31} cm^6/sec and 9.9×10^{-32} cm^6/sec, respectively. Electron and hole ionization rates are taken from [13].

• *Numerical technique*

Equations (1)–(3) with the auxiliary equations (4)–(19) are solved in two dimensions by the finite difference method. Two approaches have been discussed in the literature to solve the above equations. The first approach [2, 3] is to solve (1)–(3) separately for variables ψ, n, and p using an algorithm introduced by Gummel [14] as follows:

$$\frac{\partial}{\partial\psi} F_\psi(\psi^k, n^k, p^k)\Delta\psi^{k+1} = -F_\psi, \tag{20}$$

$$\psi^{k+1} = \psi^k + \Delta\psi^k, \tag{21}$$

$$\tilde{n}^k = n^k\cdot\exp[q\Delta\psi^{k+1}/kT], \tag{22}$$

$$\tilde{p}^k = p^k\cdot\exp[-q\Delta\psi^{k+1}/kT], \tag{23}$$

$$\frac{\partial}{\partial n} F_n(\psi^{k+1}, \tilde{n}^k, \tilde{p}^k)\Delta n^{k+1} = -F_n, \tag{24}$$

$$n^{k+1} = \tilde{n}^k + \Delta n^{k+1}, \tag{25}$$

$$\frac{\partial}{\partial p} F_p(\psi^{k+1}, n^{k+1}, \tilde{p}^k)\Delta p^{k+1} = -F_p, \tag{26}$$

$$p^{k+1} = \tilde{p}^k + \Delta p^{k+1}, \tag{27}$$

where ψ^k, n^k, p^k denote starting values and ψ^{k+1}, n^{k+1}, p^{k+1} are the updated values. $\tilde{n}$ and $\tilde{p}$ are electron and hole concentrations updated for the change in the potential. This method shows a linear convergence.

The second approach [15, 16] is to solve (1)–(3) simultaneously in a quadratically convergent Newton scheme as follows:

$$\begin{bmatrix} \dfrac{\partial F_\psi^k}{\partial\psi} & \dfrac{\partial F_\psi^k}{\partial n} & \dfrac{\partial F_\psi^k}{\partial p} \\ \dfrac{\partial F_n^k}{\partial\psi} & \dfrac{\partial F_n^k}{\partial n} & \dfrac{\partial F_n^k}{\partial p} \\ \dfrac{\partial F_p^k}{\partial\psi} & \dfrac{\partial F_p^k}{\partial n} & \dfrac{\partial F_p^k}{\partial p} \end{bmatrix} \cdot \begin{bmatrix} \Delta\psi^{k+1} \\ \Delta n^{k+1} \\ \Delta p^{k+1} \end{bmatrix} = \begin{bmatrix} -F_\psi^k \\ -F_n^k \\ -F_p^k \end{bmatrix}. \tag{28}$$

Although this approach requires much more computer storage and run time for each loop, it has been shown to converge faster for high injection bias conditions [16].

The diagonal part of (28) is the loop given by Eqs. (20), (24), and (26). The terms $(\partial F_n^k/\partial\psi)\Delta\psi^{k+1}$ and $(\partial F_p^k/\partial\psi)\Delta\psi^{k+1}$ of (28) are Eqs. (22) and (23). The terms $\partial F_n/\partial p$ and $\partial F_p/\partial n$ are mainly electron-hole recombination and generation terms, which are usually small in shallow junction devices. Therefore, to improve the convergence of the first approach without increasing computer storage requirements makes it necessary to approximate the terms $(\partial F_\psi^k/\partial n)\Delta n^{k+1} = -(q/\varepsilon)\Delta n^{k+1}$ and $(\partial F_\psi^k/\partial p)\Delta p^{k+1} = (q/\varepsilon)\Delta p^{k+1}$ of Eq. (28). This requires a prediction of Δn^{k+1} and Δp^{k+1} before solving (20) for $\Delta\psi^{k+1}$.

We have used the "Gummel" method to solve (1)–(3) with the following modifications to improve speed. As the solution is approached and the relative change in n and p at various grid points becomes small, Eqs. (25) and (27) are replaced by the following equations:

$$n^{k+1} = \tilde{n}^k + dn^{k+1}, \tag{29}$$

$$dn^{k+1} = \Delta n^{k+1} + Cdn^k, \tag{30}$$

$$p^{k+1} = \tilde{p}^{k+1} + dp^{k+1}, \tag{31}$$

$$dp^{k+1} = \Delta p^{k+1} + Cdp^k, \tag{32}$$

where C is a constant which is optimized for best convergence. Formulas (30) and (32) determine the prediction for a new n^{k+2}, p^{k+2} for use in (20) by extrapolation using the previous change in n and p. **Figure 2** shows the convergence improvement in a high injection bias solution for an npn transistor for various values of the parameter C. Values of $C = 0.4$ and 0.5 have been taken as default values for Eqs. (30) and (32), respectively.

• *Boundary conditions*

Values of variables ψ, n, and p or their normal derivatives are specified at the boundary of a two-dimensional region of analysis. Both ohmic and Schottky metal-semiconductor

contacts can be specified. At an ideal ohmic contact, carrier concentration is specified by the thermal equilibrium values [2, 3]. Boundary conditions for a Schottky contact on n-type silicon include the following thermionic emission boundary conditions for both electrons and holes:

$$J_n = (A_n^{**}T^2/N_c)(n - n_0), \tag{33}$$

$$J_p = (A_p^{**}T^2/N_v)(p - p_0), \tag{34}$$

where A_n^{**} and A_p^{**} are the effective Richardson constants for electrons and holes; n, p and n_0, p_0 are the actual and zero bias surface concentrations of electrons and holes; and N_c and N_v are the effective density of states in the conduction and valence bands, respectively. The surface electrostatic potential is fixed by the Schottky barrier to be

$$\psi = \phi_M - |\phi_B| + \frac{1}{2}|E_g|, \tag{35}$$

where ϕ_M is the metal Fermi energy, ϕ_B the barrier height, and E_g the bandgap energy.

Boundary conditions for a polysilicon-silicon interface are incorporated by a finite surface recombination velocity of minority carriers. The surface recombination velocity is introduced to simulate polysilicon-silicon interface properties and polysilicon and silicon material parameters. Its value is therefore technology-dependent. The effect of finite surface recombination velocity is numerically to modify the boundary condition for minority carriers at the contact. For an npn transistor with a polysilicon emitter contact, the hole boundary condition at the polysilicon emitter contact is specified by

$$p(x = 0) = \frac{J_p}{qS_p} + \frac{n_{ie}^2}{n(x = 0)}, \tag{36}$$

where J_p is the hole current density, n_{ie} is the intrinsic carrier concentration, $x = 0$ is the emitter polysilicon-silicon interface, and S_p is the hole surface recombination velocity at the polysilicon-silicon interface. The default value of the parameter S_p is taken as 3×10^4 cm/sec based on our technology.

• *Specification of doping profile: link with SAFEPRO*
The impurity doping profile and a two-dimensional geometry are required as input parameters for a 2DP run. Impurity doping profiles can be specified as one-dimensional profiles with associated windows. 2DP then calculates the doping profile on a two-dimensional grid using an analytical expression for elliptical fit with a specified ratio of lateral to vertical diffusion depths. Two-dimensional doping profiles of arsenic and boron impurities from a SAFEPRO run [7] can also be used for a 2DP analysis by using a software link to interpolate the doping profile from the triangular finite element grid of SAFEPRO to the rectangular finite difference grid of 2DP.

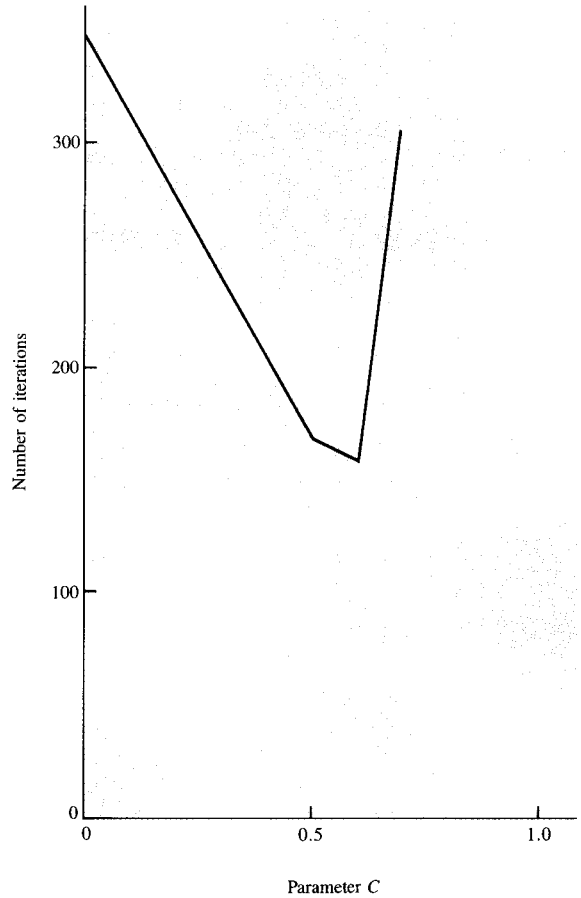

Figure 2

Number of iterations for a fixed convergence in a shallow base npn transistor simulation at high injection ($V_{BE} = 0.9$ V) bias conditions as a function of the parameter C.

Figure 3 shows a two-dimensional region of a 2DP analysis for a polysilicon-emitter, polysilicon-base npn transistor. An available arsenic and boron profile window from a SAFEPRO run is also shown in Fig. 3. The software link program takes the (X_{ref}, Y_{ref}) point as a reference and linearly interpolates the logarithm of the doping from the SAFEPRO grid to 2DP grid points. The doping profile for grid points outside the SAFEPRO window, as well as the collector profile not specified by the SAFEPRO run, is also specified by this link program. A user-oriented interactive program, with plotting capability, has been developed to specify doping profiles, grid points, and terminal bias information for 2DP analysis.

• *2DP output*
For a specified bias condition, the 2DP output on a printer, terminal, or dataset consists of an input parameter listing, the detailed device internal behavior at the grid points, and

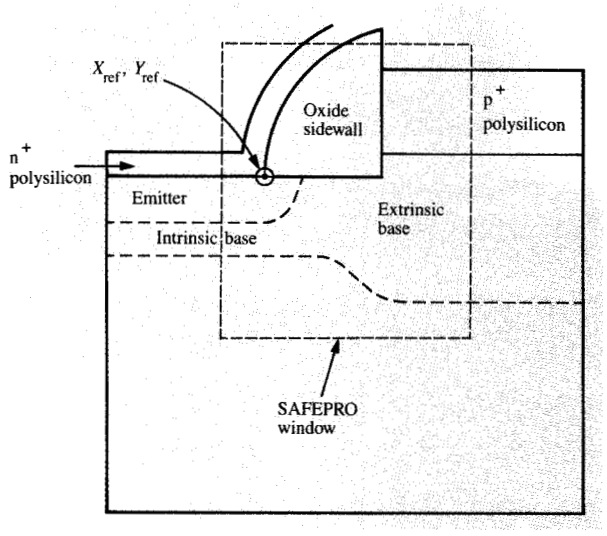

Figure 3

The two-dimensional region of analysis for a polysilicon-emitter, polysilicon-base npn transistor. The box indicates the portion of the two-dimensional profile simulated by the SAFEPRO process simulation program.

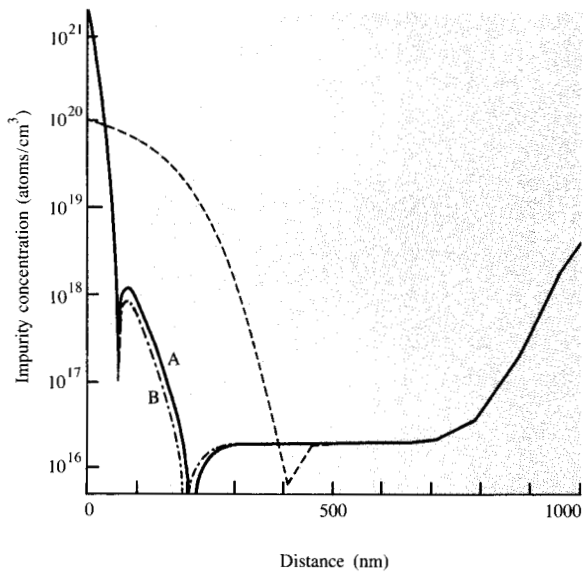

Figure 4

Vertical doping profiles for the nominal process (profile A) and 30% reduction in the intrinsic base implant dose (profile B).

terminal characteristics. In addition to terminal currents and current gain, other parameters, such as internal junction bias, sheet resistance, injection efficiency, and breakup of currents in bottom and sidewall regions, are included in the output; these are used for device equivalent circuit model construction.

If specified by the user, capacitance calculations for an npn transistor are included in the analysis after the dc solution for specified V_{BE} and V_{BC} operating conditions according to the following relations:

$$C_{BE} = \left.\frac{\partial Q_h}{\partial V_{BE}}\right|_{V_{BC}} = \left.\frac{\partial Q_e}{\partial V_{BE}}\right|_{V_{BC}}, \tag{37}$$

$$C_{BC} = \left.\frac{\partial Q_h}{\partial V_{BC}}\right|_{V_{BE}} = \left.\frac{\partial Q_e}{\partial V_{BC}}\right|_{V_{BE}}, \tag{38}$$

where C_{BE} is the capacitance due to a change in the electron charge Q_e, or the hole charge Q_h, caused by a small change of V_{BE} for constant V_{BC}; C_{BC} is the capacitance due to a change in charge storage caused by a small change in V_{BC} for a specified V_{BE}. Total capacitance values C_{BE} and C_{BC} are broken into the intrinsic (under the emitter) and extrinsic region capacitance values. Total capacitance is also divided into depletion and neutral capacitance values [17, 18] as follows:

$$C = C_n + C_s, \tag{39}$$

$$C_s = -\frac{\partial}{\partial V}\int\int \rho u(\rho)dxdy, \tag{40}$$

where C_n is the neutral capacitance, C_s is the depletion capacitance, $\rho = [N_D - N_A + p - n]$ is the net charge density and $u(\rho)$ is the unit step function. Depletion and neutral capacitance terms are further broken into intrinsic and extrinsic components for the device equivalent circuit model. The gain-bandwidth product f_t is calculated by the relation

$$f_t = \frac{1}{2\pi}\left(\frac{\Delta I_c}{\Delta Q_h}\right), \tag{41}$$

where ΔI_c is the change in collector current and ΔQ_h is the change in the stored hole charge for a small change ΔV_{BE} from specified V_{BE} and V_{BC} operating level conditions.

• *Link with MGP*

As described in detail in an accompanying paper [8], information required for a device equivalent circuit model from 2DP runs for various bias conditions is saved in a dataset. The software link program MGPLINK, for the device equivalent circuit model generation program (MGP), postprocesses these data. This program also generates plots, as shown in Figs. 4–14 of this paper.

3. Bipolar transistor simulation

The use of 2DP to design and optimize new bipolar technology device structures is illustrated in the following sections. An npn transistor structure with a 1.5×1.0-μm^2 emitter and a 4.7×1.0-μm^2 base-collector region has been

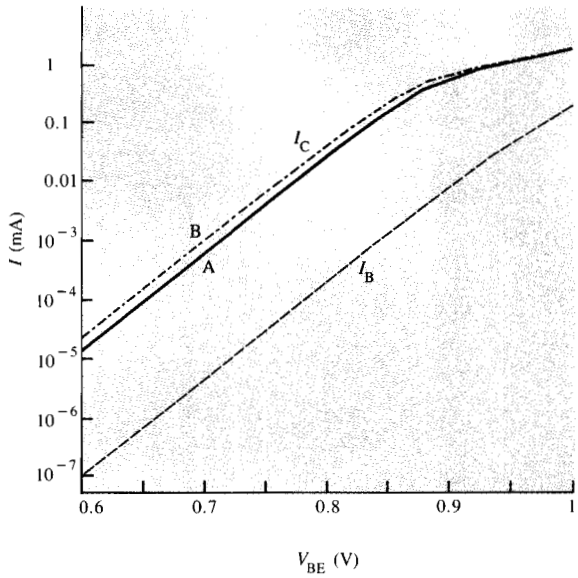

Figure 5

Predicted I_C and I_B as a function of V_{BE} for profiles A and B of Fig. 4.

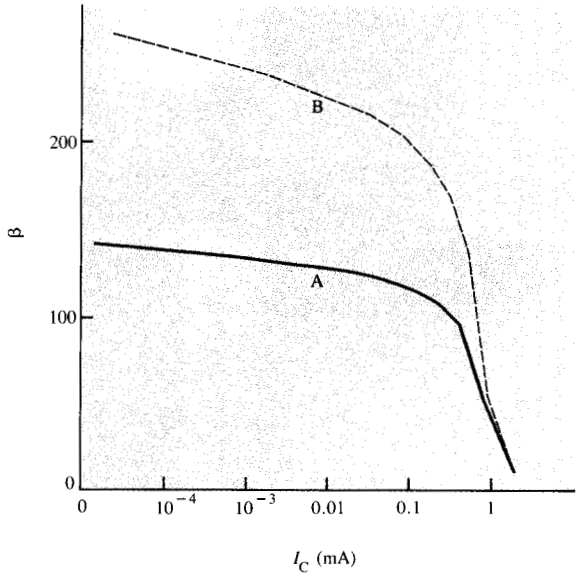

Figure 6

Current gain as a function of I_C for profiles A and B of Fig. 4.

analyzed. (The third dimension, 1.0 μm, is arbitrary since we are analyzing a two-dimensional structure.) Emitter, intrinsic base, and extrinsic base doping profiles are taken from a SAFEPRO solution described in the previous paper [7]. Epitaxial and subcollector region profiles are added to complete the specification of doping profiles for this npn transistor.

- *Base doping variation*

The first example demonstrates the effect of variations in the implanted boron dose on device characteristics. Intrinsic base profiles for the original boron dose and for a dose reduced by 30% are shown as curves A and B, respectively, in **Figure 4**. Predicted I_C, I_B vs V_{BE} characteristics for these cases are shown in **Figure 5**. As expected, I_C increases with reduced base doping. The increases in current gain and intrinsic base sheet resistivity are shown in **Figure 6** and **Figure 7**, respectively. Note that the increases in current gain and resistivity are smaller at higher currents since carrier injection dominates the built-in profile. Predicted f_t vs I_C characteristics for the two profiles are shown in **Figure 8**, where the higher base resistivity profile corresponds to the higher f_t curve due to narrower electrical basewidth and higher electron mobility.

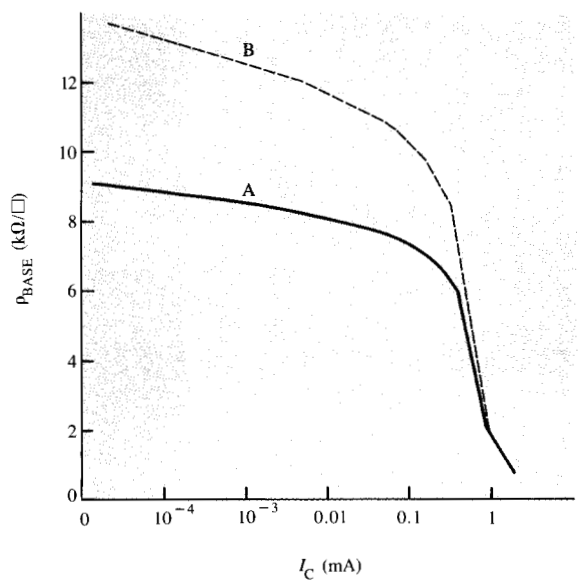

Figure 7

Intrinsic base sheet resistance as a function of I_C for profiles A and B of Fig. 4.

- *Epitaxial doping variation*

The effect of varying the epitaxial region doping level on the device characteristics is simulated by the doping profiles shown in **Figure 9**. The epitaxial doping level has been changed from 2.0×10^{16} cm^{-3} for profile A to 4.0×10^{16} cm^{-3} for profile C. Calculated emitter-base and base-collector capacitance characteristics are shown in **Figure 10**.

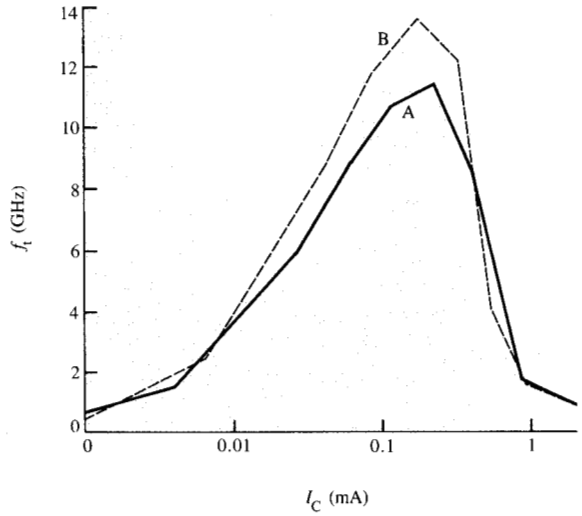

Figure 8

f_C as a function of I_C for profiles A and B of Fig. 4.

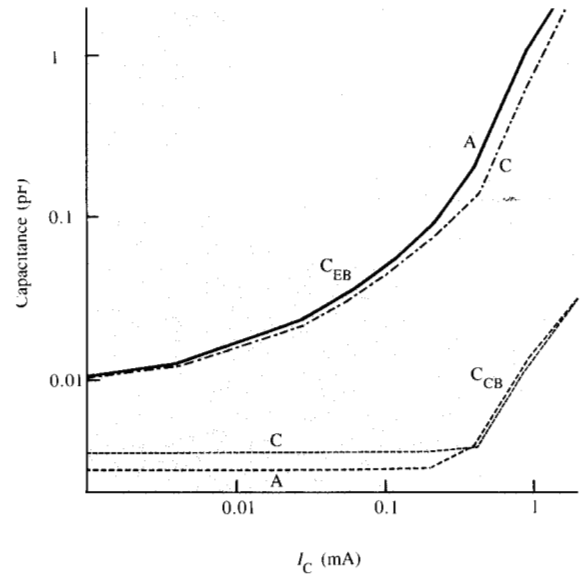

Figure 10

Emitter-base and base-collector capacitance values as a function of I_C for profiles A and C of Fig. 9.

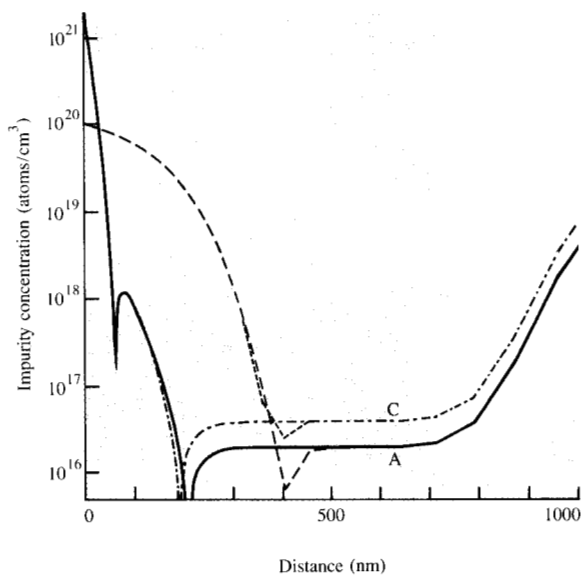

Figure 9

Vertical doping profiles for the nominal process (profile A) and for higher epitaxial region doping (profile C).

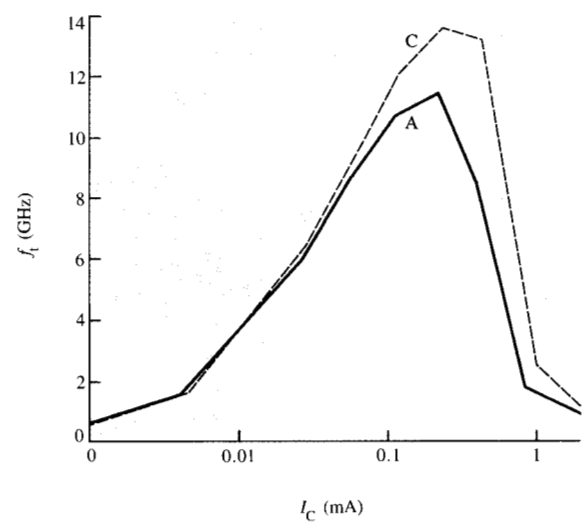

Figure 11

f_t as a function of I_C for profiles A and C of Fig. 9.

At low current levels, profile C has a higher base-collector junction depletion capacitance. However, the increase in emitter-base diffusion capacitance with increasing current level is smaller for profile C as base-widening in the epitaxial region starts at a higher current density. The effect of increased epitaxial doping is also seen in the f_t vs I_C characteristics shown in **Figure 11**, where f_t reduction with increasing I_C is smaller for profile C compared to profile A.

- *Epitaxial thickness variation*

The effect of variations in the epitaxial region thickness is simulated by considering the doping profiles shown in **Figure**

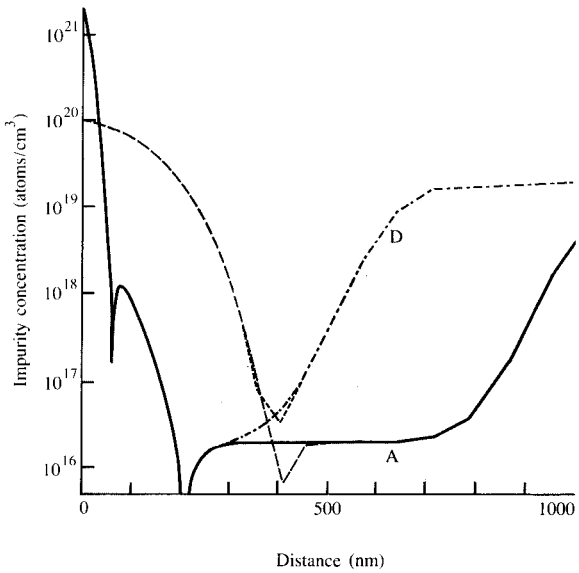

Figure 12

Vertical doping profile for the nominal process (profile A) and a reduced epitaxial region thickness (profile D).

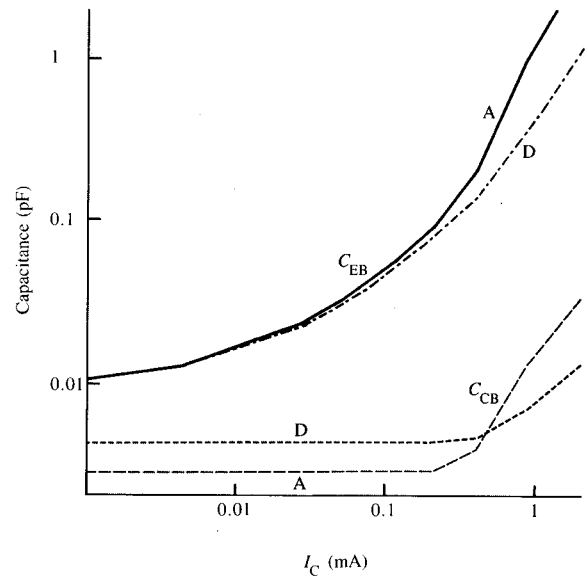

Figure 13

Emitter-base and base-collector capacitance values as a function of I_C for profiles A and D of Fig. 12.

12, where epitaxial thickness has been reduced by 400 nm for profile D. Predicted capacitance characteristics are shown in **Figure 13**, where base-collector depletion capacitance at low current levels is increased for profile D, mainly due to the higher doping level of the extrinsic base-collector junction and reduced epitaxial thickness. Due to the reduced region for base widening at high injection levels, emitter-base diffusion capacitance is smaller for profile D at high current levels. Reduced charge storage at high injection levels for profile D also accounts for higher f_t, as shown in **Figure 14**.

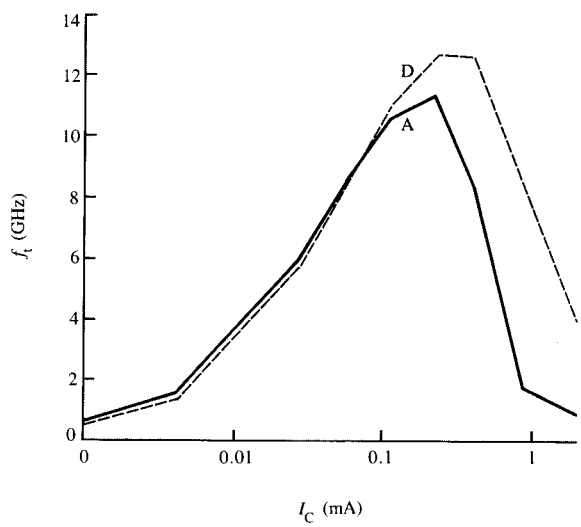

Figure 14

f_t as a function of I_C for profiles A and D of Fig. 12.

4. Summary

The mathematical details and the silicon material parameters used in the two-dimensional device simulation program 2DP have been presented. 2DP has been linked with the two-dimensional process simulation program SAFEPRO to automatically receive the two-dimensional doping profiles required for device characteristic simulation. It has also been linked with the device equivalent circuit model generation program to automatically transfer predicted terminal characteristics and device internal behavior required for equivalent circuit modeling. Use of 2DP to optimize bipolar technology device design and to estimate device characteristic variation due to process tolerances has also been discussed.

5. Acknowledgments

The user-oriented interactive program for using 2DP was written by T. Georgen and D. Johnson during their summer employment, with the help of R. Jones and P. Murley.

6. Appendix: List of symbols

A_n^{**} Effective Richardson constant for electrons

A_p^{**} Effective Richardson constant for holes

A_n Auger recombination coefficient for n-type silicon

A_p	Auger recombination coefficient for p-type silicon
C_{BC}	Base-collector capacitance
C_{BE}	Base-emitter capacitance
C_n	Neutral capacitance
C_s	Depletion capacitance
C	Extrapolation parameter for convergence optimization
E	Electric field
E_c	Critical electric field
ΔE_c	Conduction band edge change
ΔE_c^{bt}	Conduction band edge change due to band tailing effect
ΔE_c^{mb}	Conduction band edge change due to many-body effect
ΔE_v	Valence band edge change
ΔE_v^{bt}	Valence band edge change due to band tailing effect
ΔE_v^{mb}	Valence band edge change due to many-body effect
ΔE_g	Bandgap change
f_t	Gain-bandwidth product
F_ψ	Operator for Poisson's equation
F_n	Operator for electron current continuity equation
F_p	Operator for hole current continuity equation
G	Generation rate
I_B	Base current
I_C	Collector current
ΔI_C	Change in collector current after a small change in bias voltage
J_n	Electron-current density
J_p	Hole-current density
k	Boltzmann constant
n	Mobile-electron concentration
n_0	Zero bias mobile-electron concentrations
$\tilde{n}^k$	Modified mobile-electron concentration at iteration step k
n_{i0}	Intrinsic-electron concentration
n_{ie}	Effective intrinsic-carrier concentration
N	Total doping ($N_D + N_A$)
N_A	Net acceptor concentration
N_D	Net donor concentration
N_c	Effective density of states in conduction band
N_v	Effective density of states in valence band
p	Mobile-hole concentration
p_0	Zero bias mobile-hole concentration
$\tilde{p}^k$	Modified mobile-hole concentration at iteration step k
p_{i0}	Intrinsic-hole concentration
q	Electron charge
Q_e	Total electron charge
Q_h	Total hole charge
ΔQ_h	Change in stored hole charge after a small change in bias voltage
R	Recombination rate
R_{AUGER}	Auger recombination rate
R_{SRH}	Shockley-Read-Hall recombination rate
S_p	Hole surface recombination velocity at the polysilicon-silicon interface
T	Absolute temperature
T_n	Temperature normalized to 300°K
$u(x)$	Unit step function $u(x) = 1$ for $x > 0$ $u(x) = 0.5$ for $x = 0$ $u(x) = 0$ for $x < 0$
V_{BC}	Base-collector voltage
V_{BE}	Base-emitter voltage
α_n	Electron ionization rate
α_p	Hole ionization rate
β	Constant
ε	Dielectric constant
ϕ_n	Electron quasi-Fermi potential
ϕ_p	Hole quasi-Fermi potential
ϕ_B	Schottky barrier height
ψ	Electrostatic potential
μ_n	Electron mobility
μ_p	Hole mobility
ρ	Net change density
τ_{n0}	Electron lifetime parameter
τ_{p0}	Hole lifetime parameter

References

1. R. W. Knepper, S. P. Gaur, F.-Y. Chang, and G. R. Srinivasan, "Advanced Bipolar Transistor Modeling: Process and Device Simulation Tools for Today's Technology," *IBM J. Res. Develop.* **29**, 218–228 (1985, this issue).
2. S. P. Gaur and D. H. Navon, "Two-Dimensional Carrier Flow in a Transistor Structure Under Nonisothermal Conditions," *IEEE Trans. Electron Devices* **ED-23**, 50–57 (1976).
3. S. P. Gaur, "Two-Dimensional Analysis of High-Voltage Power Transistors," *IBM J. Res. Develop.* **21**, 306–314 (1977).
4. S. P. Gaur, "Performance Limitations of Silicon Bipolar Transistors," *IEEE J. Solid-State Circuits* **SC-14**, 337–343 (1979); also *IEEE Trans. Electron Devices* **ED-26**, 415–421 (1979).
5. S. P. Gaur, G. R. Srinivasan, and I. Antipov, "Verification of Heavy Doping Parameters in Semiconductor Device Modeling," *Technical Digest*, IEEE International Electron Devices Meeting, Washington, DC, December 1980, pp. 276–279.
6. Y. J. Park, R. K. Cook, and S. P. Gaur, "The Effect of Carrier Concentration Dependent Band Gap Narrowing on Bipolar Device Characteristics," *IEEE Trans. Electron Devices*, to be published.
7. R. R. O'Brien, C. M. Hsieh, J. S. Moore, R. F. Lever, P. C. Murley, K. W. Brannon, G. R. Srinivasan, and R. W. Knepper, "Two-Dimensional Process Modeling: A Description of the SAFEPRO Program," *IBM J. Res. Develop.* **29**, 229–241 (1985, this issue).
8. F.-Y. Chang and L. F. Wagner, "The Generation of Three-Dimensional Bipolar Transistor Models for Circuit Analysis," *IBM J. Res. Develop.* **29**, 252–262 (1985, this issue).
9. R. K. Cook, "Numerical Simulation of Hot-Carrier Transport in Silicon Bipolar Transistors," *IEEE Trans. Electron Devices* **ED-30**, 1103–1110 (1983).
10. Y. J. Park, D. H. Navon, and T. W. Tang, "Monte Carlo Simulation of Bipolar Transistors," *IEEE Trans. Electron Devices* **ED-31**, 1110–1116 (1984).
11. N. D. Arora, J. R. Hauser, and D. J. Roulston, "Electron and Hole Mobilities in Silicon as a Function of Concentration and

Temperature," *IEEE Trans. Electron Devices* **ED-29,** 292–295 (1982).
12. C. Jacoboni, C. Canali, G. Ottaviani, and A. Alberigi Quaranta, "A Review of Some Charge Transport Properties of Silicon," *Solid State Electron.* **20,** 77–89 (1977).
13. D. R. Decker and C. N. Dunn, "Temperature Dependence of Carrier Ionization Rates and Saturated Velocities in Silicon," *J. Electron. Mater.* **4,** 527–547 (1975).
14. H. K. Gummel, "A Self-Consistent Iterative Scheme for One-Dimensional Steady State Transistor Calculations," *IEEE Trans. Electron Devices* **ED-11,** 455–465 (1964).
15. V. C. Alwin, D. H. Navon, and L. J. Turgeon, "Time-Dependent Carrier Flow in a Transistor Structure Under Nonisothermal Conditions," *IEEE Trans. Electron Devices* **ED-24,** 1297–1304 (1977).
16. E. M. Buturla and P. E. Cottrell, "Simulation of Semiconductor Transport Using Coupled and Decoupled Solution Techniques," *Solid State Electron* **23,** 331–334 (1980).
17. F. Y. Chang, "Generalized Integral Charge Control Modeling of Bipolar Transistors: Part I: Theory," *IEEE Trans. Electron Devices*, to be published.
18. F. Y. Chang and S. F. Chu, "Statistical Modeling of Submicron, Shallow-Junction, Self-Aligned Bipolar Transistors," *Technical Digest*, IEEE International Electron Devices Meeting, San Francisco, CA, 1982, pp. 672–675.

Received October 1, 1984; revised January 4, 1985

Robert K. Cook *IBM General Technology Division, East Fishkill facility, Route 52, Hopewell Junction, New York 12533.* Dr. Cook received the A.B. and A.M. degrees, both in physics, from Dartmouth College, Hanover, New Hampshire, in 1978, and in 1981 the Ph.D. degree in electrical engineering from Cornell University, Ithaca, New York, where he was a National Science Foundation graduate fellow. Since 1981 he has been employed by the IBM General Technology Division, working in the areas of device design and characterization for high-performance bipolar integrated circuits. Since 1982 he has also been an adjunct assistant professor of physics at Vassar College, Poughkeepsie, New York. His primary research interests are in the areas of semiconductor device and materials physics, especially carrier transport processes in submicrometer structures. He was a co-recipient of the 1982 Rappaport Award from the IEEE Electron Devices Society. Dr. Cook is a member of Phi Beta Kappa.

Santosh P. Gaur *IBM General Technology Division, East Fishkill facility, Hopewell Junction, New York 12533.* Dr. Gaur received the B. Tech. degree in electrical engineering from the Indian Institute of Technology, Kanpur, India, in 1969, the M.S. degree in electrical engineering from the University of Maine at Orono in 1971, and the Ph.D. degree in electrical and computer engineering from the University of Massachusetts, Amherst, in 1974. He joined the IBM Corporation in Poughkeepsie, New York, in 1974. At present, he is managing the Device Physics Technology Department at East Fishkill. His previously published research work has been in the area of lattice vibrations and associated thermodynamic properties of III-V and II-VI compounds of zinc blende structure, numerical simulation of semiconductor devices, reliability of high-power semiconductor devices, and bipolar transistor design and optimization. He holds four U.S. patents in the area of semiconductor device fabrication. Dr. Gaur has been a member of the honorary editorial advisory board of *Solid State Electronics* since 1980. For the year 1984–85, he is serving as the Electron Devices Society Chapter Chairman in the Mid-Hudson section of the IEEE. He is a member of Eta Kappa Nu and Sigma Xi.

Peter A. Habitz *IBM General Technology Division, East Fishkill facility, Route 52, Hopewell Junction, New York 12533.* Dr. Habitz received the Ph.D. degree in theoretical chemistry from the University of Bonn, Federal Republic of Germany, in 1975. He worked for five years as a research associate at the University of Karlsruhe, Germany, on quantum-mechanical calculations of problems in pseudopotentials, spectroscopy, and molecular scattering. He joined IBM in Poughkeepsie, New York, in 1981 and performed calculations for the structure of liquid water. In 1983 he joined the Device Technology Department at East Fishkill to work on device and process simulations in order to optimize device design and to predict the effect of process changes on device performance.

Yi-Shiou Huang *IBM General Technology Division, East Fishkill facility, Route 52, Hopewell Junction, New York 12533.* Dr. Huang received the Ph.D. degree in physics from the University of Cincinnati, Ohio, in 1969. He joined the IBM Corporation in 1969 and has since worked in the areas of device design, modeling, and characterization for bipolar and MOSFET devices. He is currently working on bipolar devices in the Device Physics Technology Department at East Fishkill. Dr. Huang is a member of the Institute of Electrical and Electronics Engineers.

Young-June Park *Goldstar Semiconductor Corporation, Seoul, Korea.* Dr. Park received his B.S. in 1975 and his M.S. in 1977, both from Seoul National University, Korea, and his Ph.D. from the University of Massachusetts, Amherst, in 1983. From 1977 to 1980, he served with the Korean Navy as a faculty member of the Korean Naval Academy, where he taught physical electronics and circuit theory. In 1983, he joined the Device Physics and Technology Department at IBM East Fishkill, where he worked on the modeling, design, and optimization of advanced bipolar device structures. Dr. Park is a member of the Korean Institute of Electrical Engineers.

Lawrence F. Wagner *IBM General Technology Division, East Fishkill facility, Route 52, Hopewell Junction, New York 12533.* Dr. Wagner is an advisory engineer in the Device Design and Modeling Department. He joined the IBM General Technology Division in East Fishkill in 1981 and has since worked on the modeling of Schottky barrier diodes and bipolar transistors. Dr. Wagner received a B.S. from the Massachusetts Institute of Technology in 1960. From 1961 to 1968 he worked for the U.S. Army Electronics Command in Fort Monmouth, New Jersey, investigating the design of micropower logic circuits. Subsequently, as a National Science Foundation Fellow, he received an M.S. in 1969 and a Ph.D. in 1981 from Stanford University, California. His doctoral research included the first direct observation of silicon surface states using ultraviolet photoelectron spectroscopy. He has also completed a postdoctoral assignment at the University of Hawaii, where he modeled the angular dependence of X-ray photoelectrons. Dr. Wagner is a member of the American Physical Society, the Institute of Electrical and Electronics Engineers, and Sigma Xi.